Scanning tunneling microscopy and density functional theory study of initial bilayer growth of Ag films on NiAl(110)

Baris Unal,[1,2] Feili Qin,[3,2] Yong Han,[3] Da-Jiang Liu,[2] Dapeng Jing,[4,2] A. R. Layson,[5] Cynthia J. Jenks,[2] J. W. Evans,[6,2] and P. A. Thiel[4,1,2]

[1]*Departments of Materials Science and Engineering, Iowa State University, Ames, Iowa 50011, USA*
[2]*Ames Laboratory-USDOE, Iowa State University, Ames, Iowa 50011, USA*
[3]*Institute of Physical Research and Technology, Iowa State University, Ames, Iowa 50011, USA*
[4]*Department of Chemistry, Iowa State University, Ames, Iowa 50011, USA*
[5]*Department of Chemistry and Biochemistry, Denison University, Granville, Ohio 43023, USA*
[6]*Department of Mathematics, Iowa State University, Ames, Iowa 50011, USA*
(Received 18 June 2007; revised manuscript received 17 September 2007; published 9 November 2007)

Scanning tunneling microscopy (STM) studies of the deposition of Ag on bcc NiAl(110) in the temperature range from 200 to 300 K reveal an initial bilayer growth mode. In this regime, which encompasses at least the first two levels of bilayer islands, the film appears to have an fcc Ag(110)-like structure. Selection of this structure reflects an almost perfect lateral match between the Ag(110) and NiAl(110) lattice constants. Density functional theory (DFT) analysis of supported Ag films with an ideal fcc(110) structure on NiAl(110) indicates that the bilayer growth mode is promoted by a quantum size effect. However, the system does not exhibit perfect Ag(110) film growth. STM analysis reveals that the tops of Ag islands are decorated by a ripple structure even in the initial levels of growth and also shows a deviation from Ag(110)-like bilayer growth to Ag(111)-like monolayer growth for thick films. DFT analysis is also applied to provide some insight into the observed deviations from perfect Ag(110) film structure.

I. INTRODUCTION

There has been extensive experimental and theoretical analysis for both homoepitaxial and heteroepitaxial growth of thin metal films.[1–3] The great majority of these studies have used single-element single-crystal substrates. However, using instead intermetallics as substrates or "templates" for thin film growth provides significant additional possibilities for guiding film structure and morphology. This strategy could potentially lead to novel nanostructures with tailored properties for surface enhanced Raman spectroscopy, catalysis, magnetism, or other applications.

To explore such possibilities, in this paper, we examine the structure of Ag films grown on one such substrate, the binary alloy NiAl(110). This combination of materials is structurally intriguing because the bulk structures of the substrate and film are fundamentally different, NiAl being CsCl (bcc-like, $a_{NiAl}=0.289$ nm) and Ag being fcc ($a_{Ag}=0.408$ nm). However, there is virtually perfect in-plane lattice matching between Ag(110) and NiAl(110). This feature is illustrated in Figs. 1(a) and 1(b). Consequently, this system provides an ideal candidate in which to study morphological evolution during heteroepitaxy in the absence of a lateral mismatch strain. In particular, it is of interest to determine whether Ag adopts the fcc(110) structure atop this NiAl template.

The NiAl surface has attracted much attention in the past for several main reasons. First, NiAl is of technological importance in high-temperature applications such as turbines.[4] Second, thin layers of alumina that are both well-ordered and conductive can be grown on this surface. These layers serve as tractable models for the alumina supports common in heterogeneous catalysts.[5] Third, the electronic structure of NiAl(110) includes a small depression in the density of states at the Fermi edge.[6] This feature has led to its selection as a substrate for growth of one-dimensional atomic wires both theoretically[7] and experimentally[8–10] (the latter being formed via atomic manipulation at low temperature), with focus on fundamental electronic and magnetic traits of the wires.

As a result of this widespread interest, the NiAl surface is reasonably well characterized. As shown in Fig. 1(a), the arrangement of atoms in the (110) plane is anisotropic, consisting of rows of Ni and Al atoms in a 1:1 stoichiometry. In a previous structure determination using multiple scattering analysis of intensity-voltage variation of low-energy electron diffraction (LEED) spots,[11] the (110) surface was found to be bulk terminated, except for two features. The first was a rumpling of the top layer in which the Al atoms protrude above the Ni atoms by 0.02 nm. The second was a first interlayer expansion of a few percent (assuming that the Al atoms define the topmost plane). The structure was confirmed by medium energy ion scattering[12] and by x-ray scattering.[13] This characterization was further supported by density functional theory (DFT) calculations[7,14] and reconfirmed in our own analysis.

Numerous studies of Ag thin film growth on a variety of other substrates have been reported. From these, a few pertinent generalizations can be drawn. First, Ag films do not alloy with other transition metal substrates at room temperature. Alloying occurs in some systems, but only at temperatures of ~500 K or above.[15–31] While Ag can insert into surface planes of pure Al substrates,[32] Ag is not known to react with surfaces of alloys containing Al and earlier transition metals such as Ni or Pd at room temperature.[33,34] Presumably, this is because the Al-Ni bond is much stronger than the Al-Ag or Ni-Ag bond, as reflected in the thermody-
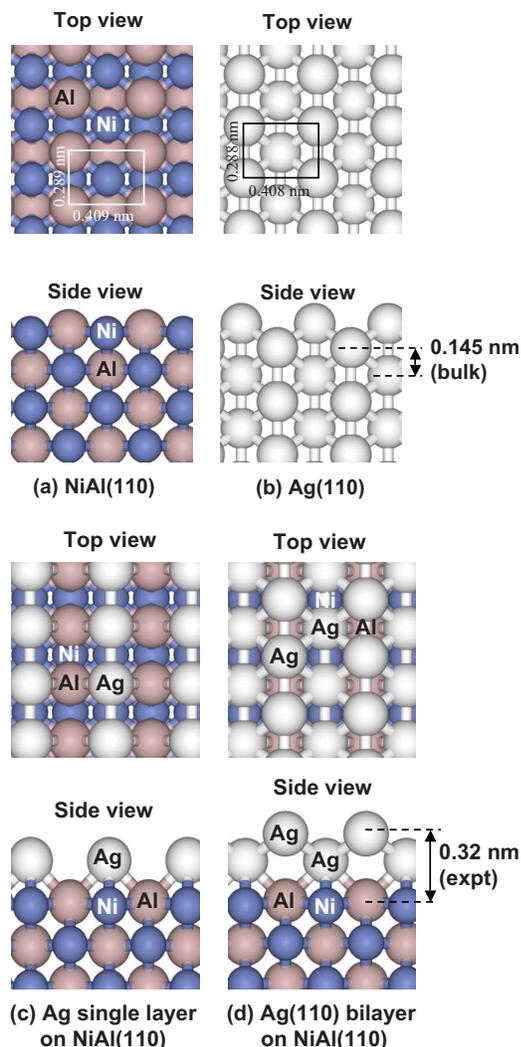
FIG. 1. (Color online) Depictions of idealized surface structures using coordinates output from DFT calculations. (a) Clean NiAl(110). (b) Clean Ag(110). (c) NiAl(110) with a monolayer of Ag. Ag adopts the Ni-bridge sites, as discussed in the Appendix. (d) NiAl(110) with two layers of Ag(110).

namic data for the respective alloys.[35–37] Thus, alloying is not anticipated in the present work, wherein Ag is deposited at 200 and 300 K. Second, the low surface energy of Ag usually leads the first few layers to "wet" the substrate, although strain can trigger three-dimensional growth in higher layers (Stranski-Krastanov growth). An example of the latter is Ag on W(110).[17,38] Finally, clean films of Ag (and also Au) that are sufficiently thick—on the order of 10–50 layers or more—tend to exhibit an fcc(111) orientation or be vicinal to the (111).[33,39–42] This tendency prevails on diverse substrates, although details of the film morphology such as twinning and defect structure may depend on the interface, and some exceptions can be found.

In Sec. II, we provide some background on our experimental procedures and on our supporting DFT calculations. In Sec. III, we present the main results of our study. First, we describe scanning tunneling microscopy (STM) observations for multilayer growth of Ag films mediated by nucleation

and growth of islands within each level. In this paper, "layer" denotes an essentially flat, low-index atomic plane, whereas "level" corresponds to islands of a specific height, labeled according to sequence of appearance with increasing Ag coverage. We will argue that two Ag(110)-like layers—i.e., a (110) bilayer—comprise each of the first two levels. We will propose that as the film thickens, a transition occurs and eventually single Ag(111)-like layers—i.e., (111) monolayers—comprise each level. DFT analyses of benchmark ideal fcc Ag(110) film structures supported on a NiAl(110) substrate are then presented together with evidence that a quantum size effect promotes the initial bilayer growth. We also describe more subtle features of growth including rippling of the tops of Ag islands. Additional DFT analysis of other film structures is presented, which elucidates the rippling and which also provides insight into the deviation from bilayer growth for thicker films. Further discussion is provided in Sec. IV. An appendix briefly describes the adsorption site of isolated Ag adatoms on NiAl(110), adatom diffusion, and the Ag-Ag interactions that lead to the observed island shapes.

II. DETAILS OF EXPERIMENTS AND CALCULATIONS

A NiAl single crystal was grown using the Bridgman technique.[43] The samples were oriented and sectioned from the ingot by electrical discharge machining. The NiAl surface was oriented to within ±0.25° of the (110) orientation and then polished using standard metallographic techniques. The polished sample was mounted on an Omicron heater and introduced into an ultrahigh-vacuum chamber equipped with Auger electron spectroscopy (AES), LEED, and STM. The base pressure of the chamber was 2×10^{-11} Torr. The sample was cleaned by repeated cycles of Ar$^+$ sputtering (20 min, 1.5 keV, and $T = 300$ K) followed by annealing to 1200 K for 2 h, until the surface was judged clean by AES, LEED, and STM. The annealing temperature corresponds to about 2/3 of the melting point, 1915 K. STM images were processed using WSXM software.[44]

STM images reveal that these sample preparation procedures can produce a NiAl(110) surface with broad terraces (up to 1 μm wide). In the data presented in this work, specifically, the terraces were up to 110 nm wide for deposition of Ag at 300 K and up to 260 nm at 200 K. The terraces were separated by monatomic steps and step bunches. Line scans across these steps indicated a step height of 0.204±0.006 nm, nearly equal to the value of 0.2014 nm expected from the bulk lattice constant of NiAl. We were thereby able to calibrate the z-piezo in the STM, a key requirement for subsequent characterization of vertical surface structure.

In thin film growth studies, Ag was evaporated from a commercial Omicron source. However, this source had a rather open design, and so we modified it with a cap containing a 1.25 mm orifice. This made the arrangement more like a true Knudsen cell. The base pressure was below 10^{-10} Torr during deposition. Flux calibration of the source was achieved by measuring the coverage directly from the STM images at low coverage. The estimated flux value was 1.6
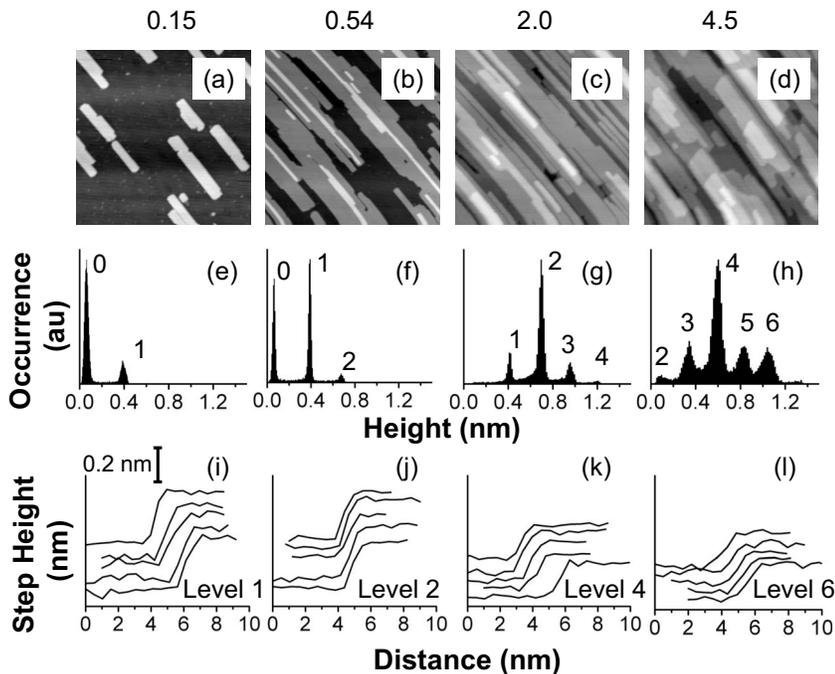
FIG. 2. STM data for Ag deposited on NiAl(110) at 200 K as a function of coverage [measured in units of Ag(110) bilayers] shown above the STM images. The top row [(a)–(d)] shows STM images of size of 100×100 nm^2. The middle row [(e)–(h)] shows pixel height histograms from a small areas of the surface corresponding to a single terrace of the substrate (and not necessarily from within the image in the top row). Peaks in the histograms are labeled with the island level. The average level is not exactly equal to the total coverage given the transition from bilayer to monolayer growth. The average level height from the histogram also depends strongly on the small area sampled, but not the step heights. The bottom row [(i)–(l)] shows representative step profiles for the levels indicated.

$\times 10^{-3}$ bilayer s^{-1} [where a bilayer is defined as two layers of a perfect Ag(110) film] for the studies conducted at a surface temperature of 300 K and 3.3×10^{-3} bilayer s^{-1} for those done at 200 K.

Some STM data are also reported for comparative studies of Ag deposition on Ag(110). These experiments were performed in a different chamber, with base pressure below 1 $\times 10^{-10}$ Torr. The Ag(110) sample was cleaned by repeated cycles of Ar$^+$ sputtering (20 min, 0.5 keV, and $T \approx 300$ K) followed by annealing at 700 K. The Ag was deposited at 220 K, and the flux was 4.5×10^{-2} monolayer s^{-1}.

For electronic structure calculations, we used DFT with the generalized gradient approximation proposed by Perdew *et al.*[45] The single-particle Kohn-Sham equations[46] were solved using the plane-wave-based Vienna *ab initio* simulation package (VASP).[47] The electron-ion interactions were described by the projector augmented-wave approach.[48] The energy cutoff for the plane-wave basis was set to be the default value for freestanding or supported Ag(110) films. The converged magnitude of the forces on all relaxed atoms was always less than 0.1 eV/nm. To prevent spurious interactions between adjacent replicas of the thin film system, we used a vacuum layer that was 1.5 nm thick in the direction perpendicular to the surface. The optimized lattice constants were 0.2896 nm for NiAl and 0.4166 nm for Ag, to be compared with the experimental values of 0.289 and 0.408 nm, respectively. These theoretical lattice constants were used in all subsequent calculations.

As background for analysis of supported Ag films on NiAl(110) presented below, some brief remarks on the DFT predictions for the structure of the clean NiAl(110) surface follow. Our DFT calculations reproduced the experimental results reasonably well. For instance, the vertical separation between surface Ni and Al atoms is 0.017 nm from our DFT [for a 21-layer NiAl(110) slab], whereas it is 0.016 nm from x-ray scattering[13] and 0.022 nm from LEED.[11] The first in-

terlayer spacing[49] is larger than the bulk value by 3.1% from our DFT, compared with (3.8 ± 0.6)% from x-ray scattering,[13] 4.6% from LEED,[11] and (5.0 ± 2.0)% from medium energy ion scattering.[12] Our calculations further showed that the surface energy of clean NiAl(110) is 1.57 J/m^2 for the fully relaxed surface. This is, as might be expected, comparable to but lower than the value obtained from a previous DFT analysis of a fixed (unrelaxed) substrate, 1.65 J/m^2.[50] Furthermore, it is higher than the surface energy of Ag(110), 1.24–1.42 J/m^2.[51,52] Hence, surface energy differences should drive Ag(110) films to grow layer by layer on NiAl(110), although this prediction is rather crude because it ignores the interfacial energy.

Finally, one might anticipate quantum size effects associated with the finite thickness of the slab of NiAl(110) substrate used in calculations below for supported Ag films. Indeed, calculations for NiAl(110) slabs of various thickness did indicate some variations of the surface energy of thin Ag films. However, in this work, comparisons are made while holding the NiAl slab thickness constant, so this effect should not impact our analysis of relative energetics associated with supported Ag films of various thicknesses.

III. EXPERIMENTAL AND THEORETICAL RESULTS FOR Ag FILMS ON NiAl(110)

A. Ag island step heights from scanning tunneling microscopy data

Figures 2 and 3 show STM images of Ag islands deposited on NiAl(110) at 200 and 300 K, respectively, for various film thicknesses [the associated coverages being reported in units of Ag(110) bilayers], together with representative information about step heights. From the STM images shown in the top row of each figure, it is clear that Ag forms two-dimensional islands. These islands are large and display
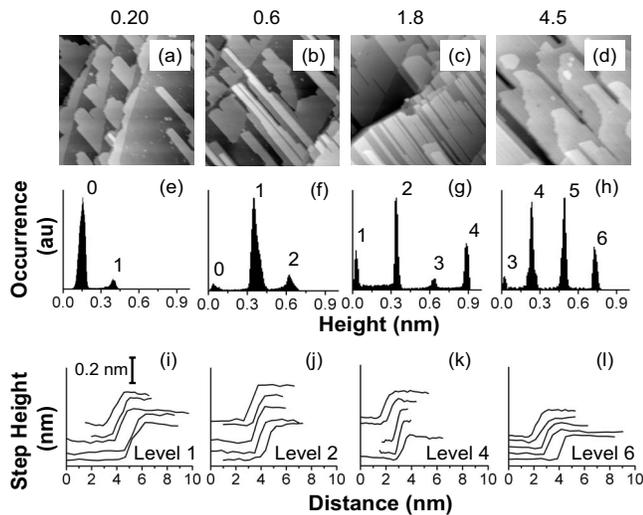
FIG. 3. STM data for Ag deposited on NiAl(110) at 300 K with increasing coverage [measured in units of Ag(110) bilayers] shown above the STM images. Top row [(a)–(d)] shows STM images of size of 100×100 nm^2, middle row [(e)–(h)] shows pixel height histograms (not necessarily from the image in the top row), and bottom row [(i)–(l)] shows representative step profiles for the levels indicated. Peaks in the histograms are labeled with the island level.
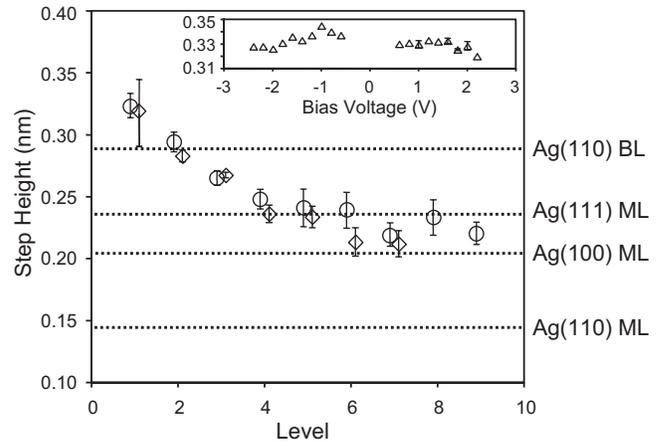

FIG. 4. Experimental step heights from pixel height histograms in STM images. Circles and diamonds show step heights at 200 and 300 K, respectively, as a function of Ag island level (lower abscissa). Each pair of data points is slightly offset from the exact value of the island level (i.e., offset horizontally) to avoid overlap. Actual values are given in Table I. The horizontal dashed lines show ideal step heights based on interplanar spacings in bulk Ag for a (110) bilayer (BL) and for various types of monolayers (ML). Triangles show step heights measured as a function of bias voltage (top abscissa) for islands in level 1.

highly anisotropic, rectangular shapes. Diffusion across terraces is sufficiently rapid at 300 K that, for a terrace width of about 100 nm or less and for the deposition rate specified above, Ag islands grow outward from steps as long fingerlike protrusions. This behavior corresponds to step flow growth. Diffusion is slower at 200 K, so that islands nucleate and grow in the middle of terraces, as well as at step edges. See the Appendix for a brief discussion of terrace diffusion of individual Ag adatoms on NiAl(110), together with the strong anisotropy in adatom interactions which produces elongated islands and the adsorption site.

Histograms of the pixel heights in a smaller region of the surface (chosen within a single terrace of the substrate) are shown in the middle row of each figure. The separations between peaks (which are labeled by the level of islands above the substrate) correspond to the average island or step heights d within the sampled region. The bottom rows show representative line profiles, from which representative values of the step heights d can also be derived. (Profiles are taken from a variety of images at different locations on the surface, not just from the images shown.) We analyze both line profiles and histograms because profiles show individual characteristics while histograms obscure individual peculiarities but provide objective average values.

As an aside, note that the average coverage quoted above the STM images does not correspond exactly to the average level of the film surface in the sampled region, where the latter can be extracted from the histograms. There are two reasons for this discrepancy. First, histograms are taken from small areas in which the local coverage can fluctuate significantly. Second, the density of Ag atoms depends on the level, as will be clear from the discussion below.

Figure 4 and Table I show average values of d, determined from histograms, for islands in different levels. The

results are virtually identical when line profiles are used. It can be seen that there is no significant difference between step heights at 200 or 300 K. The step height is 0.32 nm for the first-level islands and is 0.29 nm for the second-level islands at both temperatures. These are about twice the value expected for a Ag(110) monolayer. As the island level increases (moving higher up in the film), the step height decreases and eventually levels off in the range of 0.21–0.24 nm.

Electronic effects could influence measurements of step height. This possibility is strongest for the first-level islands, i.e., those directly atop the NiAl(110) substrate. Electronic effects can be revealed by changing the tunneling bias. A measurement of step height, for islands within the first level at 200 K, vs tunneling voltage is shown in the inset of Fig. 4. The step height of 0.32 nm does not change strongly with bias voltage, and hence we conclude that 0.32 nm is a topographic value (reflecting positions of ion cores). For higher-level islands, where growth resembles homoepitaxy, another electronic effect known as Smoluchowski smoothening could conceivably influence STM measurements if the islands were very small (containing a few tens of atoms) and closely spaced (within a few tenths of a nanometer).[53] However, the islands in our data are much too large and well separated for the Smoluchowski effect to be significant.

It is instructive to compare these Ag islands with the ones grown on the (110) surface of bulk Ag. The latter are shown in Fig. 5(a) for deposition at 220 K. Like the Ag/NiAl(110) islands, the Ag/Ag(110) islands are flat and elongated. The histogram in Fig. 5(c) reveals that they have a step height of $d = 0.15$ nm. Furthermore, this is the step height of intrinsic surface terraces on Ag(110), which is also shown by Fig. 5(b). This value of d equals the bulk interplanar spacing, 0.145 nm, as shown in Fig. 1(b).

TABLE I. Heights of majority islands, in nm, in different levels. (Examples of minority or "anomalous" islands are given in Fig. 6 and described in the text.) When two numbers are given for a single island level from STM data, the top entry is for deposition at 200 K and the bottom for 300 K. Data are provided for both height histogram and line profile analysis. For the line profiles, each entry is based on at least six profiles. In the DFT calculations, the first-level step heights are derived from the difference between the height of the ion cores of the top Ag atoms and the average height of the ion cores of the Ni and Al atoms in the top substrate layer.

Island level	STM histograms	STM line profiles	DFT of Ag(110) bilayer films on NiAl(110)
1	0.324 ± 0.010	0.334 ± 0.027	0.340
	0.317 ± 0.027	0.324 ± 0.027	
2	0.294 ± 0.008	0.292 ± 0.012	0.290
	0.283 ± 0.005	0.282 ± 0.013	
3	0.265 ± 0.006	0.263 ± 0.017	0.295
	0.267 ± 0.002	0.254 ± 0.017	
4	0.248 ± 0.008	0.248 ± 0.020	0.294
	0.236 ± 0.007	0.242 ± 0.018	
5	0.241 ± 0.015	0.237 ± 0.019	0.293
	0.234 ± 0.009	0.237 ± 0.020	
6	0.239 ± 0.014	0.234 ± 0.018	0.294
	0.213 ± 0.012	0.233 ± 0.024	
7	0.220 ± 0.010	0.225 ± 0.010	0.293
	0.212 ± 0.011	0.225 ± 0.013	
8	0.233 ± 0.014	0.224 ± 0.017	0.294
9	0.221 ± 0.009	0.215 ± 0.020	0.292

The step height for Ag/Ag(110) is about half of the value for the first- and second-level islands of Ag/NiAl(110). Whereas Ag islands on bulk Ag(110) form single layers, we propose that Ag islands on NiAl(110) are essentially Ag(110) bilayers, at least in the first two levels. The structure of a Ag bilayer of Ag(110) on NiAl(110) is illustrated in Fig. 1(d), and for completeness, the structure of a Ag(110) monolayer is illustrated in Fig. 1(c).

As noted above, the average island height decreases as island level increases. At the high-coverage limit, the heights of the Ag islands, 0.21–0.24 nm, are bracketed by those expected for Ag(111), 0.236 nm, or Ag(100), 0.204 nm, but are significantly larger than the step height of Ag(110), 0.145 nm. This indicates that bilayer growth does not continue and that the atomic structure is not that of perfect Ag(110) in the higher-level islands. Specifically, we propose that there is a transition from Ag(110)-like bilayer growth to Ag(111)-like monolayer growth. See also Sec. III D.

Finally, it should be noted that islands are sometimes observed within the second level, which does not fit the above description. These are illustrated in Fig. 6. These anomalous islands are always 2 nm wide, and they range in length from about 5 to 30 nm. We find them only within the second
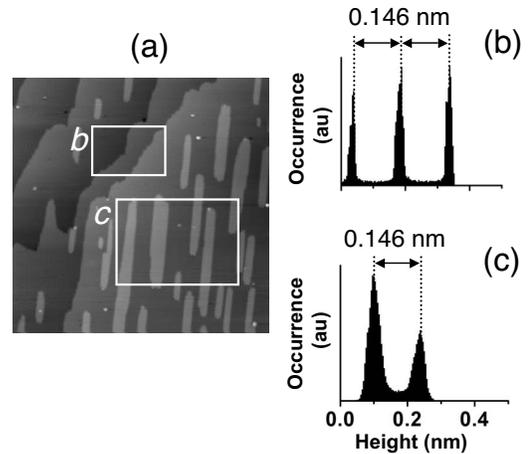

FIG. 5. (a) STM image of Ag deposition on Ag(110) at 220 K. The Ag coverage is 0.3 monolayer, image size is 270×270 nm², scanning current is 0.3 nA, and scanning voltage is +1 V. (b) Histogram of pixel heights from area *b* in (a), encompassing two terrace step edges. (c) Histogram of pixel heights from area *c* in (a), encompassing several islands on a single terrace.

level. They are 0.09–0.11 nm higher than the surrounding Ag surface constituting the top of first-level islands. Very occasionally, they merge with normal (higher and wider) bilayer islands, as in Fig. 6(d). In such a case, the width of the anomalous island is still 2 nm but its height is about 0.14 nm. These single-layer Ag islands may serve as precursors to the bilayer within the second level.

B. Benchmark density functional theory studies of structure and energetics for an ideal fcc Ag(110)/NiAl(110) film: Rational for initial bilayer growth

We have performed extensive DFT calculations to assess the energetics of ideal Ag(110) films of various thicknesses on the NiAl(110) substrate. In the surface free energy calculations, we used a (1×1) lateral unit cell, thus enforcing perfect lateral periodicity. We used $15 \times 15 \times 1$ *k* mesh. Ag atoms in the first layer are located at the site between Ni
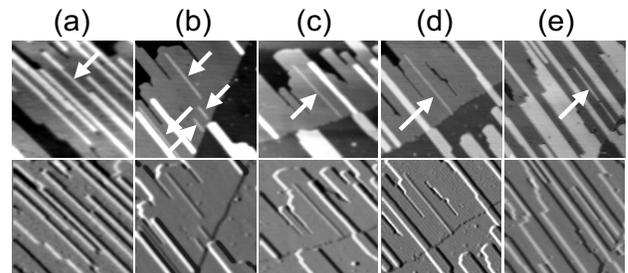

FIG. 6. Examples of anomalous islands, indicated by arrows, following deposition of Ag at 200 K. These are atop first-level islands. In (a), one of these islands bridges two regions with "normal" step heights, illustrating its likely origin as a Ag(110) monolayer. In each vertical pair, the top frame is the normal constant current image, and the bottom frame is the differentiated version. Each image is 50×50 nm².
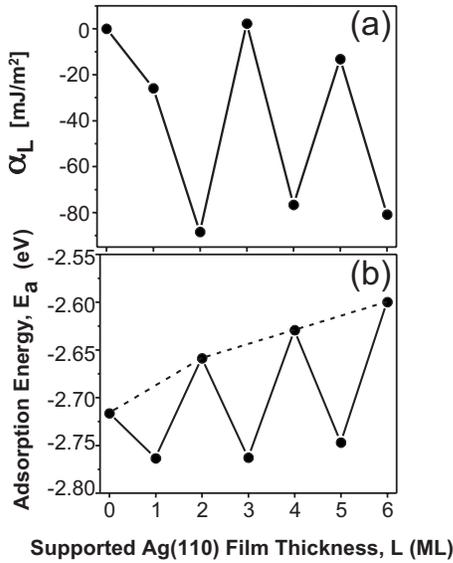
FIG. 7. (a) DFT calculation of α_L as a function of Ag(110) film thickness L. The Ag films are supported by a five-layer NiAl(110) slab. (b) DFT calculation of adsorption energy E_a as a function of Ag(110) film thickness L. The Ag films are supported by a four-layer NiAl(110) slab. The dashed line connecting the maxima indicates that the adsorption energy becomes progressively less favorable on higher bilayers.

atoms of the substrate, the preferred binding site for isolated Ag adatoms on this surface. (See the Appendix.) The structure of the NiAl(110) surface changes very little when these Ag(110) films are added. This feature has been checked for films on a five-layer NiAl(110) slab with the bottom layer fixed. At the interface, there is still the rumpled NiAl structure similar to that of the freestanding NiAl(110) surface mentioned in Sec. I. As the Ag(110) film grows thicker (from 1 to 22 layers), the distance between the top-layer Al atom center and its nearest Ag atom center decreases from 0.203 nm and converges to 0.199 nm. The interlayer spacing between two Ag(110) layers is close to the calculated bulk value of 0.147 nm.

From an evaluation of the stability of ideal Ag(110) films as a function of thickness, DFT provides a rationale for bilayer growth. The quantity that best reflects the stability of the film as a function of its thickness in layers L is

$$\alpha_L \equiv \gamma_t + \gamma_b + \gamma_i - \gamma_{t,0} - \gamma_{b,0} = \frac{E_L - E_0 - N_L E_c}{A}. \quad (1)$$

Here, γ_t, γ_b, and γ_i are the free energies of the top surface, bottom surface, and interface, respectively. Generally speaking, all three energies are functions of film thickness. E_L is the total energy including the NiAl substrate, N_L is the total number of Ag atoms in the added L layer Ag film, E_c is the cohesive energy per atom of bulk fcc Ag, and A is the surface area. The subscript "0" corresponds to no Ag layer on the substrate. In our analysis, total energies (free energies at zero temperature) are calculated starting with a five-layer NiAl(110) slab as the substrate with the bottom layer fixed and adding layers of Ag(110). Figure 7(a) shows the result-

ing α_L vs L for the first three bilayers. Oscillations with bilayer period develop and persist to thicker films together with some beating (not shown). It is clear that the most stable configurations (corresponding to minima in α_L) occur when films are two, four, and six layers thick.

The quantity α_L describes the energetics of an *extended* surface of a Ag(110) film supported on NiAl(110). One should also ask whether the adsorption or binding energy, $E_a < 0$, of an individual, *isolated* Ag atom on perfect Ag(110) films of various thicknesses L would oscillate similarly. This would be relevant to the initial stage of formation of each new bilayer. The relevant calculations are performed using a (2×3) lateral unit cell with a $6 \times 4 \times 1$ k mesh. In order to make the computation more efficient, the NiAl substrate is decreased to four layers in contrast to the above calculations, tests showing that this does not affect the basic results.

Figure 7(b) reveals that the adatom adsorption energy indeed oscillates with a two-layer periodicity. These oscillations persist for thicker films (not shown). Comparing the values at the minima and maxima shows that it is significantly more favorable for an adatom to adsorb atop the first Ag layer ($L=1$) than atop the NiAl(110) substrate ($L=0$). It is significantly more favorable to adsorb atop layer $L=3$ than layer $L=2$ and to absorb atop layer $L=5$ than layer $L=4$, etc. This underlies the tendency for bilayer growth. Furthermore, adsorption on higher even-numbered layers (corresponding to $L=2,4,6$) is progressively less favorable than on the NiAl(110) substrate [the maxima in Fig. 7(b) connected by a dotted line move to higher values]. This naturally leads each successive level of Ag to wet the surface, in accord with the crude surface energy arguments of Sec. II.

The oscillations in α and E_a are promoted by a quantum size effect (QSE). This effect originates from quantum confinement of electrons in the vertical direction within the Ag film when the structural dimensions of a film become comparable to the mean free path of electrons. More specifically, the stability pattern of a metal film depends on satisfying a matching condition involving the Fermi wavelength λ_F and the film interlayer spacing d.[54] If λ_F and d satisfy the condition $jd = i\lambda_F/2$, where j and i are integers, then the film will exhibit an oscillating stability with j-layer oscillation when $j \neq i$ and no oscillation when $j = i$. For a Ag(110) film, $d = 0.145$ nm and $\lambda_F = 0.5228$ nm. Then, when $i=1$, $j=1.8$, which is close to the integer 2. This indicates that the Ag(110) film has a primary stability oscillation with a period of two layers, in agreement with the DFT results for the first few layers.

The step heights calculated for the Ag(110) bilayers are shown in Table I. At the fourth bilayer, the step height has reached the asymptotic limit for thick films, 0.294 nm. For the first two levels, theory agrees well with experiment, supporting the interpretation that they are epitaxial Ag(110) bilayers. At and especially beyond the third level, however, there develops a significant difference between calculation and experiment. This suggests that there is a transition from the QSE-stabilized structure to a different one at higher levels. See Sec. III A.

C. Ripples on the upper surface of the Ag(110) film

Rather than displaying the "ideal" Ag(110) structure in the first two levels, the upper surface of the Ag islands exhibits a
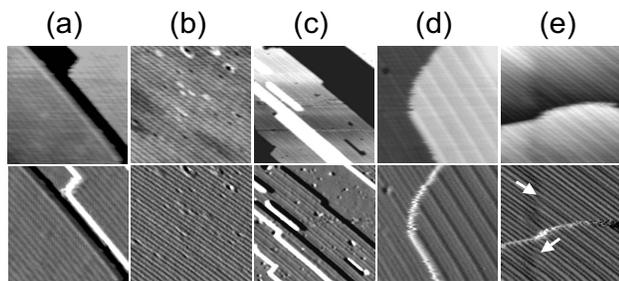
FIG. 8. Examples of ripples in the Ag islands at various levels. The top row shows images in the constant current mode, which makes depressions distinguishable from protrusions. The bottom row shows images that have been differentiated, which makes the ripples more identifiable. Each image is 23×23 nm^2. (a) First level, 300 K, depressions with period 1.2 nm. (b) First level, 300 K, depressions with period 0.8 nm. (c) First level, 200 K, depressions with both 0.8 and 1.2 nm periods. (d) Third and fourth levels, 300 K, 3.3 nm protrusions, plus depressions. (e) Fifth and sixth levels, 300 K, mixed periods with dislocations. The dislocations form a vertical column in the image. The white arrows point to two examples.

FIG. 9. DFT predictions for the rippled structure of a Ag(110) bilayer of periodicities (a) $n=2$ and (b) $n=3$. To make the rippling visible, all deviations (of all species, in all directions) from the unrippled bilayer Ag(110) atom positions are magnified by a factor of 10. Open circles are Ag, darkest circles are Ni, and light gray circles are Al.

lateral structure consisting of linear ripples or stripes. Such features also occur in higher levels which do not have Ag(110) structure (as surmised above based on their step heights). This ripple or stripe feature is shown in Fig. 8. The stripes can be divided into two groups on the basis of their appearance and separation. The first types are imaged as depressions, i.e., dark lines, about 0.02 nm deep and either 0.8 or 1.2 nm apart. These depressions are illustrated in Figs. 8(a) and 8(b). The second type appears as protrusions, i.e., bright lines, about 0.02–0.05 nm high and separated by 3.3 nm [Fig. 8(d)]. Between these protrusions, depressions are usually visible. Ripples separated by other distances, such as 1.8, 2.3, and 2.6 nm, can also be found, but they are uncommon. The ripples develop as a function of increasing film height or level. The depressions appear in the first level, but the 3.3 nm protrusions appear only in upper levels. Ripples are aligned across island steps, as is obvious in Figs. 8(d) and 8(e).

Our DFT analysis of ideal Ag(110) film structures in Sec. III B used a (1×1) lateral unit cell, thus enforcing lateral periodicity and excluding rippling. However, we have also performed a less restrictive DFT analysis which indicates that depressions in the first level could be due to a slight spontaneous rippling in the fcc(110) bilayer structure, i.e., rippling is not incompatible with and might reasonably be expected for perturbed Ag(110) bilayer structures. These additional DFT calculations were performed using $(n \times 1)$ supercells, placing $2n$ Ag atoms (to represent the first-level islands) on top of a slab of six layers of NiAl(110) substrate. The first five layers of the substrate were allowed to relax.

For $n=2$ (with a period 0.82 nm), a rippled structure with an amplitude of 0.009 nm is found. This structure is energetically more favorable than the unrippled one by 2 meV per unit cell. With $n=3$ and therefore a period of 1.23 nm, a rippling consisting of two rows of high Ag separated by one row of lower Ag atoms is found. The amplitude is again
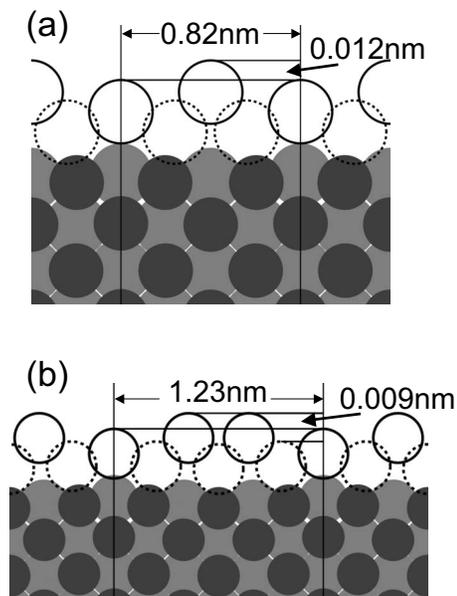
about 0.009 nm. The structure is favored by about 0.9 meV per unit cell over the flat structure. See Fig. 9 for side views for $n=2$ and $n=3$. With $n=4$, aside from a period 0.82 nm rippled structure (trivially obtained from two of the above-mentioned $n=2$ structures), another (metastable) structure with 1.64 nm periodicity and even larger ripples can be found. However, it is less favored than the flat structure. For the $n=2$ and $n=3$ structures, the periods of the ripples are in good agreement with those observed experimentally, and the amplitude of the rippling agrees to within a factor of 2. One cannot give a simple unambiguous identification of the dominant driving force for rippling, but one might note that while the lateral mismatch between the substrate and Ag(110) film is small, there is significant strain inherent in the different crystal structures of the two materials (bcc-like vs fcc).

Of course, one should not expect DFT to reliably predict such small energy differences between the unrippled and rippled structures. However, the calculations do show that it is plausible for rippled structures to have slightly lower energies. Note that the effect on determining film structure of this small energy difference per unit cell is cumulative: for Ag films with long islands or rows of atoms, the energy difference between an unrippled and a rippled structure per row is the energy difference per atom times the length of the row. Furthermore, since the topological difference between the flat and rippled structures is very small, one can argue that there is very little (if any) energy barrier for the transition between them, so the system will easily find the rippled structure if it is indeed more energetically favorable. The fact that both separations (0.8 and 1.2 nm) are observed in experiment indicates that there is a competition between the
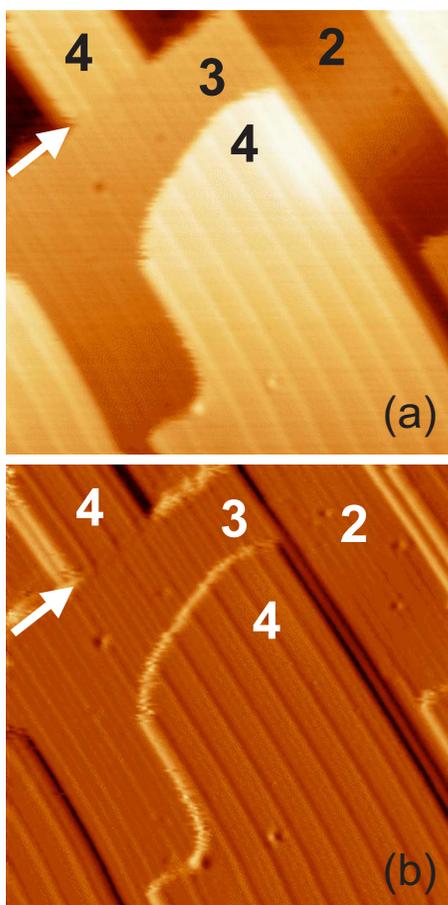
FIG. 10. (Color online) Development of protrusion ripples in levels 2, 3, and 4 of Ag films. At the arrow, the Ag film crosses a NiAl step and, consequently, the Ag island level increases from 3 to 4. The image size is 51×51 nm^2. (a) Constant current image (0.5 nA, +1 V). (b) Differentiated image.

two, which may be affected by factors such as defects or growth history.

Since we do not have a detailed model for the structure of the Ag film above the first two bilayers, it is more difficult to characterize the 3.3 nm protrusions that appear on higher terraces. The amplitude of these ripples seems to increase gradually from the second level to the fourth; in the fourth and higher levels, their amplitude is constant at about 0.05 nm. The progression with level height is illustrated in Fig. 10, where one of the Ag islands crosses a step edge at the arrow. Different levels are labeled numerically. The 3.3 nm protrusions are clearly more pronounced on the fourth-level Ag islands than on the third-level island, and least of all on the second-level island. Hence, the development of the 3.3 nm protrusions seems to correlate with the decrease in step height (and transition from bilayer to monolayer growth) shown in Fig. 4 and Table I. That is to say, in levels 2–4, the step height decreases and the protrusions develop in parallel. At and above level 4, both features are constant.

D. Other structures of the Ag film

We should emphasize that for initial Ag film growth on NiAl(110), our DFT calculations indicate that there is not a strong energetic driving force preferring the Ag(110) structure over all other structures. Indeed, there are a variety of monolayer structures composed of local hexagonal, i.e., Ag(111)-like, and square, i.e., Ag(100)-like, motifs for which we find that DFT actually predicts a lower energy per atom than the Ag(110) structure (although the energy difference is only ~0.02 eV/atom). However, these structures do not match the experimentally measured island or step heights. Assuming that these structures do actually have lower energy than Ag(110)-like films (which is unclear given the uncertainty in DFT predictions), one must conclude that their formation is kinetically hindered relative to that of Ag(110) films. In this regard, we have found that the lowest energy position for a single Ag atom adjacent to a complete row of Ag atoms on the substrate is at the bridge site between two Ni atoms in the Ag(110) position, rather than in a closer threefold hollow position compatible with alternative denser structures. Thus, it is plausible that nucleation and growth of the Ag(100) structure are favored, and conversion to another structure is inhibited.

We have also performed additional DFT analysis to explore specific aspects of the stability of Ag(110) bilayer islands. We describe two such analyses here.

(i) We have analyzed the single bilayer Ag(110) structure with even larger $(n \times 1)$ lateral unit cells than described in Sec. III C. These calculations have revealed that for $n \geqslant 4$, it is energetically favorable for the bilayer structure to convert to a structure with a higher density of atoms in the first layer than in the second layer. However, transition to such a structure from a perfect or slightly rippled (with lateral period of 0.82 or 1.23 nm) bilayer (110) structure is generally activated, perhaps providing a rationale for why these structures are not realized, according to our proposed model, for the initial stages of film growth.

(ii) We have also performed a DFT analysis to explore the structure of Ag(110) bilayer islands of finite width. Here, we found a tendency for atoms in the first layer in a narrow island to contract laterally. This contraction provides the driving force for the above-mentioned rippled structures and potentially for Ag(111)-like domain walls between Ag(110) regions.

Next, we consider the structure of thick films. As indicated above, our STM studies for prolonged growth reveal that ultimately, thick Ag films on NiAl(110) appear to develop a Ag(111)-like structure. For a 40-layer film grown at 300 K, we find that islands are more isotropic compared with the highly elongated islands observed for thin films. The island edges are also faceted, with facets frequently displaying the 120° angles expected for a Ag(111)-like hexagonal structure. These features are shown clearly in Fig. 11.

Perhaps the most complicated aspect of growth is the transition from initial Ag(110) bilayer growth to the ultimate Ag(111)-like monolayer growth. If the initial growth did have an ideal Ag(110) structure, then it would be more difficult to rationalize the transition away from this structure given the lack of lateral mismatch in this system. However,
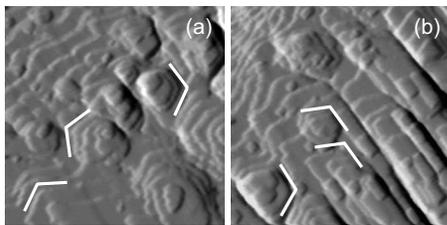
FIG. 11. [(a) and (b)] STM images of a Ag film, about 40 layers thick, on NiAl(110) at 200 K. Several sets of 120° angles are illustrated with the white lines. The images have been differentiated to accentuate the step edges. Each image size is 100×100 nm^2.

we have shown in Sec. III C that the film never has an ideal Ag(110) structure, displaying rippling even in the lowest levels. This initial rippling feature and perhaps the effect of substrate defects (such as deviations from stoichiometric surface composition, buried dislocations, and steps) could all produce perturbations from the ideal Ag(110) structure that might grow with film thickness. This could naturally lead to a reduction with increasing film height of the barrier to the development of non-Ag(110) structures, and thus ultimately lead to the formation of the Ag(111)-like structure.

IV. SUMMARY AND DISCUSSION

The main outcome of the present investigation is the finding that Ag films grow in a Ag(110) bilayer mode on NiAl(110), at least in the first two levels. The tendency for bilayer growth of these films is promoted by a QSE. The QSE, in turn, reflects a barrier to electron propagation at both the Ag-vacuum and Ag-NiAl interfaces.

Formation of bilayer islands on the nanometer scale has been observed in some other metal on metal film growth systems in the initial submonolayer stages of deposition. These systems include Ag/Fe(100),[55,56] Co/Cu(111),[57,58] Au/Ag(110),[59] and Fe/Cu$_3$Au(001).[60] Several mechanisms have been suggested to drive such bilayer growth including magnetostriction effects, a combination of strain and exchange processes, and QSE. A surfactant can also force bilayer growth.[61] Sometimes, there is a barrier to the formation of bilayer islands which restricts their nucleation to steps, or near to steps, on the surface.[56,58] One could easily conclude that a terrace nucleation barrier exists here as well if only data at 300 K were available, but the 200 K data prove that is not true, in the Ag/NiAl(110) system. Instead, preferential nucleation at steps at 300 K here is due to heteroepitaxial step flow, i.e., preferential Ag atom capture at existing steps due to rapid diffusion across terraces on the time scale of deposition.

Many other systems have been reported to exhibit QSEs.[62,63] Usually, the film is a low-melting metal or semimetal, the most common ones being Ag, Cu, Pb, and Bi. Substrates are semiconductors (Si and GaAs) and higher-melting elemental metals (Ni, Fe, Co, and V). Additionally, quasicrystals (a type of intermetallic) can support QSEs.[64] Usually, these substrates have a gap or a pseudogap that serves to confine valence electrons within the film. In the

present case, the existence of a barrier at the Ag-NiAl interface can be rationalized similarly in terms of the small reduction in the electron density of states at the Fermi edge in NiAl(110).[6] Note also that in the electronic growth model, the period of oscillation depends on the Fermi surface; the two-layer period observed here is a feature specific to the details of the Ag/NiAl(110) system.

Finally, we reiterate the particularly appealing feature of the Ag/NiAl(110) system which both motivated and facilitated this study: the almost perfect lateral match between the NiAl(110) substrate and Ag(110) film. As noted above, this allows analysis of heteroepitaxial growth in the absence of a strong lateral mismatch strain. However, it also leads to the formation of an interface between substrate and film with a simple and natural structure amenable to detailed high-level theoretical analysis of the supported films (which is not possible for some more complex metal-on-semiconductor or metal-on-quasicrystal systems).

APPENDIX: BINDING SITES AND DIFFUSION BARRIERS FOR ISOLATED Ag ADATOMS ON NiAl(110)

We have performed a fairly comprehensive DFT evaluation of the potential energy surface for the adsorption or binding energy (as a function of lateral position) of an isolated Ag adatom on NiAl(110). This analysis shows that the most favorable adsorption site is at the bridge site between two nearest-neighbor Ni atoms, as shown in Fig. 1(c). In these calculations, the adsorption energy is defined as $E_a = E_{tot} - E_{slab}$, where E_{tot} is the total energy of the slab plus the adatom and E_{slab} is the total energy of the slab without the adatom. In calculating E_a, we use a 2×3 supercell with $4 \times 4 \times 1$ k mesh. The result is $E_a = -2.72$ eV for this Ni-bridge site. The next-most-favorable site is the quasithreefold site that lies slightly off center from the Al-bridge site, defined by a triangle of Al-Al-Ni, where $E_a = -2.52$ eV. The determination of the Ni bridge as the favored site for Ag adsorption agrees with the experimental result of Wallis *et al.*, derived from atomically resolved STM.[65] Our DFT analysis also indicates that the barrier for diffusion of Ag between the Ni-bridge sites is about 0.27 eV [either in the direction parallel or perpendicular to the Ni rows shown in Fig. 1(a)].

It is not immediately clear why the Ni-bridge site should be favored over the Al-bridge site. For fcc(100) surfaces of pure Al and Ni, our DFT calculations show that the adsorption energies of Ag adatoms at fourfold hollow sites are essentially identical, i.e., −2.80 eV on Al vs −2.78 eV on Ni. For the (111) faces, Ag actually prefers Al, the binding energy at threefold hollow sites being −2.32 eV on Al vs

−2.12 eV on Ni. These calculations use the true physical lattice constants for the Ni and Al surfaces. However, if we use a single bulk lattice constant (the average of the two, 0.378 nm) to make a comparison that is more relevant to the bimetallic alloy, then on the fcc(100) faces, the binding preference is reversed: the binding energy is 0.31 eV lower (more negative) on Ni than on Al. If this difference is pro-rated according to the number of metal atoms at the adsorption site, then on NiAl(110), one expects Ag to prefer the Ni-bridge site by about 0.15 eV, close to the calculated value of 0.20 eV. We therefore suggest that the site preference is very sensitive to the Ni-Ni (or Al-Al) separation at the alloy surface.

Finally, we briefly remark on the extension of these DFT analyses to Ag adatom pair interactions. Not surprisingly, one finds a much stronger attractive interaction between Ag on neighboring Ni-bridge sites aligned with the Ni rows rather than orthogonal to these rows. This explains the tendency for islands to be strongly elongated in the direction of the Ni rows, analogous to the elongation of Ag islands on Ag(110) in the direction of the rows of Ag in the top surface layer.

[1] J. W. Evans, P. A. Thiel, and M. C. Bartelt, Surf. Sci. Rep. **61**, 1 (2006).

[2] H. Brune, Surf. Sci. Rep. **31**, 121 (1998).

[3] R. Q. Hwang and M. Bartelt, Chem. Rev. (Washington, D.C.) **97**, 1053 (1997).

[4] V. K. Sikka, S. C. Devvi, S. Viswanathan, R. W. Swindeman, and M. L. Santella, Intermetallics **8**, 1329 (2000).

[5] J. Libuda and H.-J. Freund, Surf. Sci. Rep. **57**, 157 (2005).

[6] S.-C. Lui, M. H. Kang, E. J. Mele, E. W. Plummer, and D. M. Zehner, Phys. Rev. B **39**, 13149 (1989).

[7] J. Hong, Phys. Rev. B **73**, 092413 (2006).

[8] N. Nilius, T. M. Wallis, and W. Ho, Science **297**, 1853 (2002).

[9] N. Nilius, T. M. Wallis, M. Persson, and W. Ho, Phys. Rev. Lett. **90**, 196103 (2003).

[10] M. Persson, Phys. Rev. B **70**, 205420 (2004).

[11] H. L. Davis and J. R. Noonan, Phys. Rev. Lett. **54**, 566 (1985).

[12] S. M. Yalisove and W. R. Graham, Surf. Sci. **183**, 556 (1987).

[13] X. Torrelles, F. Wendler, O. Bikondoa, H. Isern, W. Moritz, and G. R. Castro, Surf. Sci. **487**, 97 (2001).

[14] M. H. Kang and E. J. Mele, Phys. Rev. B **36**, 7371 (1987).

[15] T.-H. Kim, B.-Y. Choi, Y. J. Song, W. G. Park, S.-J. Kahng, and Y. Kuk, Phys. Rev. B **67**, 233401, (2003).

[16] H. Roder, R. Schuster, H. Brune, and K. Kern, Phys. Rev. Lett. **71**, 2086 (1993).

[17] C. Deisl, E. Bertel, M. Burgener, G. Meister, and A. Goldmann, Phys. Rev. B **72** 155433 (2005).

[18] D. B. Danko, M. Kuchowicz, R. Szukiewicz, and J. Kolaczk-iewicz, Surf. Sci. **600**, 2258 (2006).

[19] T. Valia and M. Milun, Surf. Sci. **315**, 81 (1994).

[20] M. Pivetta, F. Patthey, and W.-D. Schneider, Surf. Sci. **532**, 58 (2003).

[21] H. Noro, R. Persaud, and J. A. Venables, Surf. Sci. **357**, 879 (1996).

[22] M. Parschau, D. Schlatterbeck, and K. Christmann, Surf. Sci. **376**, 133 (1997).

[23] D. Schlatterbeck, M. Parschau, and K. Christmann, Surf. Sci. **418**, 240 (1998).

[24] T. Ito, K. Umezawa, and S. Nakanishi, Appl. Surf. Sci. **130–132**, 497 (1998).

[25] S. Nakanishi, K. Umezawa, M. Yoshimura, and K. Ueda, Phys. Rev. B **62**, 13136 (2000).

[26] R. Schuster, H. Roder, K. Bromann, H. Brune, and K. Kern, Phys. Rev. B **54**, 13476 (1996).

[27] M. Batzill and B. E. Koel, Europhys. Lett. **64**, 70 (2003).

[28] G. A. Attard and D. A. King, Surf. Sci. **222** 360 (1989).

[29] K. L. Man, Y. J. Feng, and M. S. Altman, Phys. Rev. B **74**, 085420 (2006).

[30] P. Pervan and M. Milun, Surf. Sci. **264**, 135 (1992).

[31] R. Fisher, T. Fauster, and W. Steinmann, Phys. Rev. B **48** 15496 (1993).

[32] V. Fournée, J. Ledieu, T. Cai, and P. A. Thiel, Phys. Rev. B **67**, 155401 (2003).

[33] V. Fournée, T. C. Cai, A. R. Ross, T. A. Lograsso, J. W. Evans, and P. A. Thiel, Phys. Rev. B **67**, 033406 (2003).

[34] V. Fournee, A. R. Ross, T. A. Lograsso, J. W. Evans, and P. A. Thiel, Surf. Sci. **537**, 5 (2003).

[35] S. S. Lim, P. L. Rossiter, and J. E. Tibballs, CALPHAD: Comput. Coupling Phase Diagrams Thermochem. **19**, 131 (1995).

[36] L. Hammer, H. Graupner, V. Blum, K. Heinz, G. W. Ownby, and D. M. Zehner, Surf. Sci. **412/413**, 69 (1998).

[37] *Phase Equilibria, Crystallographic and Thermodynamic Data of Binary Alloys*, edited by O. Madelung and B. Predel, Landolt-Börnstein, New Series, Group IV, Vol. 5A (Springer, Berlin, 1991).

[38] E. Bauer, H. Poppa, G. Todd, and P. R. Davis, J. Appl. Phys. **48**, 3773 (1977).

[39] K. Reichelt and H. O. Lutz, J. Cryst. Growth **10**, 103 (1971).

[40] V. Y. Aristov, M. Bertolo, K. Jacobi, F. Maca, and M. Scheffler, Phys. Rev. B **48**, 5555 (1993).

[41] G. Neuhold, L. Bartels, J. J. Paggel, and K. Horn, Surf. Sci. **376**, 1 (1997).

[42] K.-J. Chao, Z. Zhang, P. Ebert, and C. K. Shih, Phys. Rev. B **60**, 4988 (1999).

[43] Single crystals synthesisized at the Materials Preparation Center. See www.mpc.ameslab.gov

[44] I. Horcas, R. Fernandez, J. M. Gomez-Rodriguez, J. Colchero, J. Gomez-Herrero, and A. M. Baro, Rev. Sci. Instrum. **78**, 013705 (2007).

[45] J. P. Perdew, K. Burke, and M. Ernzerhof, Phys. Rev. Lett. **77**, 3865 (1996).

[46] W. Kohn and L. J. Sham, Phys. Rev. **140**, A1133 (1965).

[47] G. Kresse and J. Hafner, Phys. Rev. B **47**, 558 (1993).

[48] G. Kresse and D. Joubert, Phys. Rev. B **59**, 1758 (1999).

[49] Note that the location of any layer is potentially complicated by rumpling. The experimental studies (Refs. [11]–[13]) do not detect rumpling in the second NiAl layer, only the first. The interlayer

spacing is usually taken from experiment as the distance between the second layer and the plane containing the topmost Al atoms. In DFT, we find a rumpling in the second layer of 0.003 nm, which would probably be undetectable by experiment and which has a very small effect on the interplanar spacing. In DFT, we take the first interplanar spacing as the separation between adjacent planes of Al atoms.

[50] V. M. Kuznetsov, R. I. Kadyrov, and G. E. Rudenskii, J. Mater. Sci. Technol. **14**, 320 (1998).

[51] L. Vitos, A. V. Ruban, H. L. Skriver, and J. Kollár, Surf. Sci. **411**, 186 (1998).

[52] M. J. Mehl and D. A. Papaconstantopoulos, Phys. Rev. B **54**, 4519 (1996).

[53] P. Bedrossian, B. Poelsema, G. Rosenfeld, L. C. Jorritsma, N. N. Lipkin, and G. Comsa, Surf. Sci. **334**, 1 (1995).

[54] F. K. Schulte, Surf. Sci. **55**, 427 (1976).

[55] D.-A. Luh, T. Miller, J. J. Paggel, M. Y. Chou, and T.-C. Chiang, Science **292**, 1131 (2001).

[56] K. L. Man, Z. Q. Qiu, and M. S. Altman, Phys. Rev. Lett. **93**, 236104 (2004).

[57] J. Ferrón, L. Gómez, J. J. de Miguel, and R. Miranda, Phys. Rev. Lett. **93**, 166107 (2004).

[58] H. W. Chang, F. T. Yuan, Y. D. Yao, W. Y. Cheng, W. B. Su, C. S. Cheng, C. W. Lee, and W. C. Cheng, J. Appl. Phys. **100**, 084304 (2006).

[59] P. Fenter and T. Gustafsson, Phys. Rev. B **43**, 12195 (1991).

[60] A. Verdini, L. Floreano, F. Bruno, D. Cvetko, A. Morgante, F. Bisio, S. Terreni, and M. Canepa, Phys. Rev. B **65**, 233403 (2002).

[61] C. Deisl, K. Swamy, E. Bertel, G. Meister, and A. Goldmann, Surf. Sci. **600**, 2900 (2006).

[62] M. Milun, P. Pervan, and D. P. Woodruff, Rep. Prog. Phys. **65**, 99 (2002).

[63] M. C. Tringides, M. Jalochowski, and E. Bauer, Phys. Today **60** (4), 50 (2007).

[64] V. Fournée, H. R. Sharma, M. Shimoda, A. P. Tsai, B. Unal, A. R. Ross, T. A. Lograsso, and P. A. Thiel, Phys. Rev. Lett. **95**, 155504 (2005).

[65] T. M. Wallis, N. Nilius, and W. Ho, J. Chem. Phys. **119**, 2296 (2003).